Towards an ab-axis giant proximity effect using ionic liquid gating

Atesci, H.

Chapter 7

Etched junctions

In this chapter a new method of making (quasi) ab-axis Josephson junctions is explored, for which bilayers of $YBa_2Cu_3O_{7-\delta}/La_{2-x}Sr_xCuO_4$ are used. Etching away the top layer ensures that the flow of electrons between both $YBa_2Cu_3O_{7-\delta}$ leads is through the $La_{2-x}Sr_xCuO_4$ area. The results show first indications of a long-range proximity effect.

7.1 Introduction

Since its discovery, cuprate high-temperature superconductivity continues to be a field of interest in condensed matter physics. Several questions are still unanswered, most notably the pseudogap phenomenon. The characteristic energy gap present in cuprate superconductors persists above the critical temperature T_c. Although the nature of the pseudogap is under debate, the most prominent interpretations are that it results from, first, a pairing of the charge carriers with the superconducting coherence being suppressed due to phase fluctuations [240], or, second, a gap structure of spin/charge density wave order that competes with superconductivity [241]. Interestingly, junctions made of a cuprate barrier material in its pseudogap phase have shown anomalous properties in the form of an extended Meissner state [7], and most notably the giant proximity effect (GPE)[6, 18, 20] leading to Josephson coupling many orders of magnitude larger than the nominal coherence length [5, 6]. While many interpretations have been proposed [20, 42], the question remains whether the GPE can be related to pseudogap physics and more specifically whether a statement can be made regarding the importance of phase coherence in the pseudogap state.

Until now, *c*-axis junctions have made the compelling cases in the experimental tests of this effect. The advantage is that these can be grown without secondary-phase participates and with an rms roughness below the thickness of the barrier material. For example, in junctions formed between superconducting $La_{2-x}Sr_xCuO_4$, with a barrier made from the undoped compound La_2CuO_4 [6, 7], supercurrents have been observed for barrier thicknesses up to 10 nm, roughly two orders of magnitude larger than the c-axis coherence length ξ_c, i.e. $0.1 - 0.2$ nm. The coherence length in the coplanar axes, ξ_{ab}, is typically in the order of a nanometer, which in principle could lead to a supercurrent preservation over a distance of several hundred nanometers [6, 242]. Hence, for such distances, the strict design and interface roughness criteria that hold for the *c*-axis geometry no longer are present. Although there have been many reports of *ab*-axis GPE [13, 14, 16], most of the devices were suspected to be plagued by microshorts [243, 244], leading to ambiguous findings of the GPE in this junction geometry.

The typical *ab*-axis junction geometry initially employed grain boundaries grown on bilayer crystals [245], or ramp junctions [246]. More recently, focused He-ion beam techniques [247] have been used

to change the superconducting (S) properties of $YBa_2Cu_3O_{7-\delta}$ and induce superconductivity at a lower $T_{c'}$ (S'), or metallic (N) and insulating (I) properties. Combined with advanced lithographic techniques[248], the authors of Ref. 247 have shown to successfully produce SNS or SIS Josephson junctions. This was done with a 500 pm wide ionized beam, ensuring much smaller widths of the junction needed for SNS/SIS ab-plane configurations, as the $YBa_2Cu_3O_{7-\delta}$ coherence length in this configuration is ~ 2 nm. Interestingly, while the authors were able to decrease the T_c of the barrier material at will by adjusting the dose of the ion bombardment and hence make $SS'S$ junctions, they do not mention whether such a junction configuration induces any long range coherence lengths. Whereas the authors of Ref. 247 have used He-ion beam to change the properties of the layer into S', where S' is the same material, we have a bottom layer S' which is a different material than the top S layer. Ion irradiation (Ar+ instead of He+) is then used to completely remove the top S layer to end up with a $SS'S$ junction. More specifically, the ion irradiation is applied for bilayers of $La_{2-x}Sr_xCuO_4/YBa_2Cu_3O_{7-\delta}$ and we report supercurrent preservation in a quasi $ab-$axis geometry of ion etched junctions over distances of ~ 50 nm. Magnetic field measurements support the Josephson junction-type behavior of the devices.

7.2 Experimental details

Obtaining a giant proximity effect through etched bilayers requires a few conditions to be met. Firstly, a $T_{c'}$ should be present in the bottom film, which preferably should be as low as possible. Secondly, the T_c of the top layer should be as high as possible. Hence, bilayers have been made by (1) making use of bottom layers of less-than-optimal Sr levels (i.e. 0.09) of $La_{2-x}Sr_xCuO_4$ and (2) making use of $YBa_2Cu_3O_{7-\delta}$ as the top layer, as $YBa_2Cu_3O_{7-\delta}$ is known to have a substantially higher T_c than $La_{2-x}Sr_xCuO_4$ (bulk values of 93 K [133]), with which ΔT_c can be maximized. The T_c difference between both layers is then exploited by creating a junction that effectively removes the top layer locally by dry etching.

The bilayers are grown by means of pulsed laser deposition (PLD) with a KrF excimer laser on $LaSrAlO_4$ substrates (miscut angle of 0.2 degrees). The lattice mismatch (+0.5 %) facilitates layer-by-layer growth of the initial $La_{2-x}Sr_xCuO_4$ layer (see Fig. 7.1a(top)), mon-

itored by reflection high energy electron diffraction (RHEED). The deposition of which is done with at 740 C at an O_2 pressure of 1.3×10^{-1} mbar and a laser fluence of 1.3 J/cm^2 at 4 Hz. The growth is maintained until the completion of the 30^{th} unit cell (UC). The growth of $La_{2-x}Sr_xCuO_4$ is followed by that of $YBa_2Cu_3O_{7-\delta}$. The latter is grown at a slightly higher temperature and oxygen background pressure, 780 C and 2.0×10^{-1} mbar, respectively. Growing $YBa_2Cu_3O_{7-\delta}$ at a lower temperature near 720 C stimulates *a*-axis growth of $YBa_2Cu_3O_{7-\delta}$, which is unwanted. The laser fluence is 1.3 J/cm^2 with a repetition rate of 1 Hz, while the target-substrate distance is held at 50 mm. As can be seen in Fig. 7.1a, the clear oscillations for the first layer facilitated by a 2D growth mode are suppressed considerably with the growth of $YBa_2Cu_3O_{7-\delta}$, suggesting a 3D growth mode for this second layer. RHEED oscillations are typically unobservable after the completion of the 4^{th} UC, accompanied by a spotty RHEED pattern. The $3D$ growth is likely due to limited mobility of the ablated material on arrival at the substrate surface [167]. After deposition, the bilayer is left at 700 C for 15 min at deposition pressure, followed by an oxygen annealing treatment at 600 and 450 C, both for 30 min at a cooldown rate of 10 K/min. The $YBa_2Cu_3O_{7-\delta}$ surface is coarsened (the typical roughness is around 1.4 nm, whereas the substrate roughness is 0.3 nm), and it is possible to see unit cell step heights on the surface of the 3D islands (see Fig. 7.1b).

The deposition steps of the bilayer are shown schematically in Fig. 7.2 a,1,2. This is followed by a Au deposition process at 100 C for minimal contact resistance (Fig. 7.2 a,3), as introduced in Chapter 6. The subsequent processing step involves spinning a layer of photoresist (Fig. 7.2 a,4) which is used to mask off a part of the Au (Fig. 7.2 a,5) against the subsequent wet etching process of the exposed Au by a $KI/I_2/H_2O$ solution (4:1:40 mass ratio) (Fig. 7.2 a,6). The residual photoresist is removed by a short rinse in an ethanol and aceton bath (Fig. 7.2 a,7). Next, the sample covered is by a PMMA layer (Fig. 7.2 a,8), and a small part of it, coinciding with the red areas in Fig. 7.2 b, is exposed to an electron beam and developed (Fig. 7.2 a,9). The sample is then Ar ion milled using an acceleration voltage of 500 V. The PMMA layer, being 240 nm thick, acts as an ion stopping layer and only the developed areas are etched away in the process (Fig. 7.2 a,10) and a subsequent aceton and ethanol rinse step (Fig. 7.2 a,11)

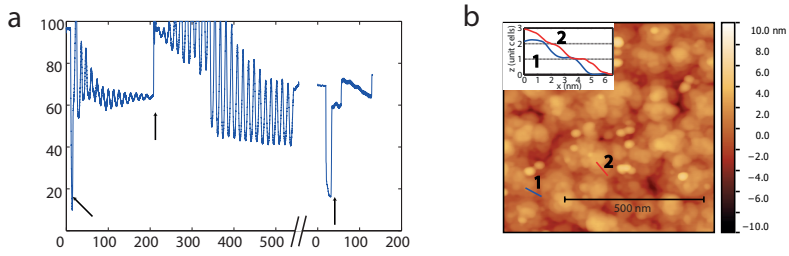

Figure 7.1: **(a)** RHEED specular intensity vs. time of 30 UC (60 RHEED oscillations) growth of $La_{1.91}Sr_{0.09}CuO_4$ and 6 UC of $YBa_2Cu_3O_{7-\delta}$. The initial $La_{1.91}Sr_{0.09}CuO_4$ grows layer-by-layer, as is indicated by the relatively large amplitude of the RHEED oscillations and the presence of the initial RHEED spots after completion of the layer. The growth of $YBa_2Cu_3O_{7-\delta}$ is characterized by a relatively small amplitude of the RHEED oscillations. The initial spots disappear and are replaced by transmission spots in the diffraction pattern, which indicate a coarsened surface. The arrows indicate the moments of electron beam current amplification, and the switch from deposition of $La_{1.91}Sr_{0.09}CuO_4$ to $YBa_2Cu_3O_{7-\delta}$ takes place at the break in the horizontal axis. **(b)** A typical AFM image of a bilayer film. The film is coarsened, with individual islands locally showing step heights corresponding to the $YBaCu_3O_{7-\delta}$ c axis lattice parameter, 11.7 Å.

concludes the sample fabrication process. The etch depth is homogeneous for all junctions being 32 ± 1 nm. Note that the ion irradiation also damages a volume extending beyond the etched volume, possibly making the $SS'S$ junction quasi planar, meaning that the current between both electrodes has a c-axis component along with its ab-axis component.

7.3 Experimental results and discussion

We observe an $R(T)$ which shows two superconducting transition temperatures, coinciding with the upper and lower layers of the bilayer. This shows that the supercurrent between both $YBa_2Cu_3O_{7-\delta}$ leads (34 nm) goes through the $La_{1.91}Sr_{0.09}CuO_4$ layer (39 nm). In the example shown in Fig. 7.3b, even though the etched depth is smaller than the thickness of $YBa_2Cu_3O_{7-\delta}$, the non-superconducting $YBa_2Cu_3O_{7-\delta}$ extends several nm beyond the etched depth due to ion irradiation damage, marked as red in Fig. 7.3b. The observation of two T_cs suggests that this non-superconducting layer extends into the bottom layer. Furthermore, some of the lower UCs of $La_{1.91}Sr_{0.09}CuO_4$

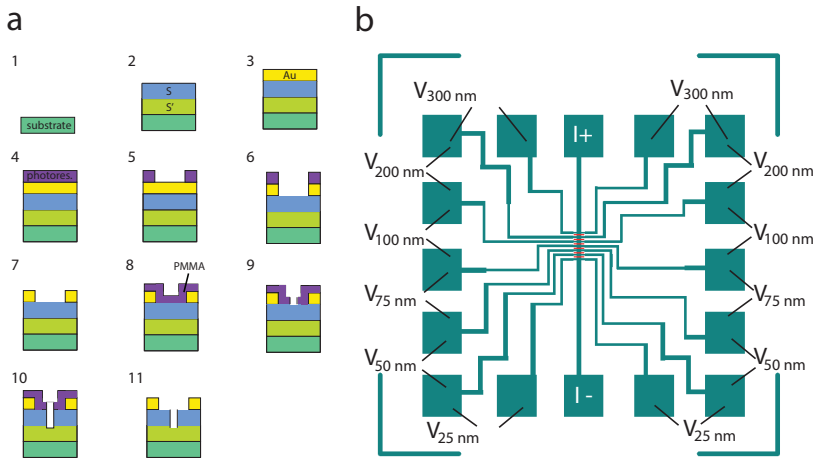

Figure 7.2: **(a)** Fabrication steps of quasi-coplanar etched junctions. 1) An initial substrate is used to 2) grow the bilayer of $La_{1.91}Sr_{0.09}CuO_4$ (S') and $YBa_2Cu_3O_{7-\delta}$ (S), followed by 3) in-situ deposition of Au. 4,5,6,7) Photolithographic and wet etching techniques are used to open up the channel area. 8,9) A subsequent electron beam lithographic process is used to write and develop the junction areas. 10,11) A final Ar ion etching process is used to etch the exposed area. 11) A final aceton and ethanol rinse step is used to remove any lithographic residuals on the surface. **(b)** Photolithographic mask design of the sample used in the fabrication process. The red areas are exposed to the electron beam in a separate process. The chip in this example contains 7 junctions of nominal widths 25 nm, 50 nm, 75 nm, 100 nm, 200 nm, and 300 nm, that are formed in the S superconductor that extends from the I^- to the I^+ lead. The labels at the other contact pads indicate the positions of the voltage probes at either side of a junction of given width.

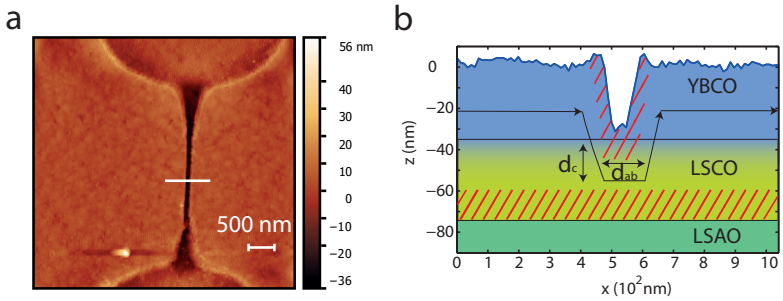

Figure 7.3: **(a)** AFM image of a typical ion milled junction geometry. The electrodes make contact with the top layer of $YBa_2Cu_3O_{7-\delta}$(the elevated plateaus left and right in the image). The gap between in the center of the image has a length of approximately 5 μm and the width slightly varies, having its narrowest part in the middle, which in this case is 47 nm wide over a length of approximately 3 μm long. The height profile of the white bar is shown in **(b)**. The etched depth is 30±1.0 nm in this case, which means that the $YBa_2Cu_3O_{7-\delta}$ is not completely removed. The volume of non-superconducting material as modified by the ion bombardment, however, extends up to and beyond the $YBa_2Cu_3O_{7-\delta}/La_{1.91}Sr_{0.09}CuO_4$ interface, shaded as red. The first UCs of bottom layer are also non-superconducting due to strain effects, which is illustrated by the red shading as well. The critical current of the leads in such a setup has both an *c*- and *ab*-axis components, indicated as d_c and d_{ab}.

are non-superconducting as well due to strain relaxation effects, estimated to be $d_{LSCO} \sim 10$ UC = 20 nm. This estimate is based on experimental data of strained $La_{1.91}Sr_{0.09}CuO_4$ films on $LaSrAlO_4$, which are semiconducting at least up to 7 UCs (see Section 3.3.4). Hence, the estimated *c*-axis depth (d_c) of the supercurrent path is between 0 and 20 UCs of the bottom layer, i.e. 26 nm. Future experiments aimed at obtaining the exact number should be done by using the same Ar ion method at $La_{1.91}Sr_{0.09}CuO_4/LaSrAlO_4$ films that are sufficiently thick. The change in critical current density then is representative of the effective reduced thickness of the superconducting layer of the film.

In Fig. 7.4a an $R(T)$ is shown for a junction width of 100 nm that is representative for the curves corresponding to all used junction geometries. The inset depicts $dR/dT(T)$ of the $R(T)$ to indicate the superconducting transition temperatures. The lower T_c measured as $d^2R/dT^2 = 0$ of 6.9 K agrees with that of $La_{1.91}Sr_{0.09}CuO_4$, while the upper T_c resembles that of $YBa_2Cu_3O_{7-\delta}$. The $R(T)$ dependence

for $T \leq$25 K is shown in Fig. 7.4b. We observe a remarkable junction width dependence of the T_c, depicted in the inset of Fig. 7.4b. For the 300 nm wide junction, $T_c = 6.8$ K, while the narrowest junction of 50 nm has the highest T_c of 9.0 K.

Next, the lowest T_c of 6.8 K is taken as a fair representation of the intrinsic T_c of the $La_{2-x}Sr_xCuO_4$ layer, which we will indicate as T_1. Although the mask design does not offer the capability to do reference measurements, these were performed separately on 7 $La_{2-x}Sr_xCuO_4$ layers of the same doping, thickness and preparation methods, which show similar values of T_c of 6.3±2.2 K. The modulation of the T_c in the junctions is taken as an anomalous effect. The anomalous effect is most pronounced for the 50 nm junction, having a $T_c = T_2$ of 9.0 K and a critical current of the junction that is 30 times larger than the critical currents observed in the wider junctions of 100 nm and 300 nm at 1.6 K.

The enhanced coupling between both superconducting leads over 50 nm is exceptional, even in a quasi-planar junction geometry. More specifically, the total path is approximately $2d_c + d_{ab}$, with d_c and d_{ab} the perpendicular and lateral distances of the current path, respectively. Although, d_c is unknown, $d_{ab} \approx 50$ nm ($\sim 20\xi_{ab}$) (see Fig. 7.3b). A more realistic value is larger than 50 nm due to ion damage not only in the lateral direction.

In experiments on junctions formed by only ion bombardment of $YBa_2Cu_3O_{7-\delta}$ [17], similar anomalous results were found over an array of Josephson junctions over distances of up to 960 nm. The authors claimed that the results might be explainable by enhanced Josephson coupling through percolating superconducting islands between two superconducting leads that are separated by a a distance much longer than the coherence length [36, 249]. The chain of superconducting islands might form a single Josephson junction, much like a percolative form of transport.

In contrast, for our bilayer junctions the role of a percolation path is much less likely, as all junctions show two superconducting transitions, which indicates that the flow of electrons goes through both layers. However, if some superconducting $YBa_2Cu_3O_{7-\delta}$ remains and forms a percolation path, one would expect to see a higher T_c for the shorter junction. The etched depth for the various junction geometries is identical within 1 nm, making this option unlikely, but not an impossibility.

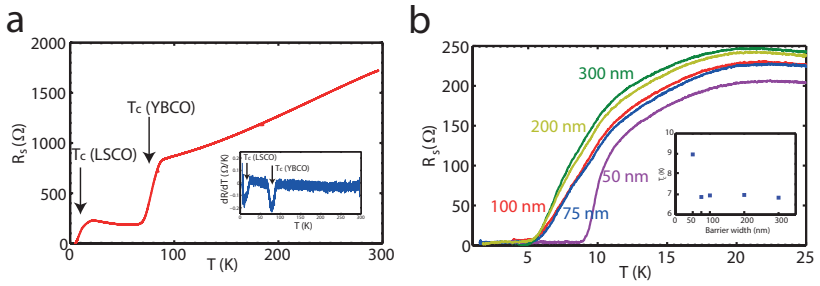

Figure 7.4: **(a)** $R_s(T)$ curve across a 100 nm wide junction which shows two transition temperatures of $La_{2-x}Sr_xCuO_4$ (LSCO) and $YBa_2Cu_3O_{7-\delta}$ (YBCO), as is indicated in the inset by the $dR/dT(T)$ curve. **(b)** $R(T)$ curve for $T \leq 25$ K for used junction geometries. The inset shows T_c given by $d^2R/dT^2 = 0$ as a function of junction width.

We aim to test whether the effect can be attributed to homogeneous Josephson coupling by means of magnetic field dependence of the critical current through the junction. The measurements were performed for the 50 and 300 nm wide junctions, with the magnetic field oriented perpendicular to the plane of the layers the data of which is shown in Fig. 7.5a. For a rectangular geometry and a homogeneous coupling we expect an oscillatory behavior in the critical current as a function of the magnetic field as a result of phase difference between both superconducting leads (Fraunhofer pattern) [250]. Measured values of the critical current for these measurements were done using a 1μV criterion. The expected oscillation period ΔB is equal to $\Delta B = \Phi_0/A$. Here, Φ_0 is the magnetic flux quantum and A is the junction area. Based on AFM images, the junction geometry is estimated to be 47 nm$\times$5 μm, leading to $\Delta B \sim$8 mT.

For $T \leq T_1$ the complete bilayer is superconducting, and no oscillatory behavior is to be expected as no phase difference is formed between both ends of the junction. The behavior that is observed shows a persistent critical that is reduced by only about a factor of 2 at 20 mT for both widths of the junction (for the 50 nm junction the data below T_1 are only shown for positive fields). Remarkably, a different type of behavior is seen for the 50 nm junction that also has the enhanced T_c, and only in the range for $T_1 \leq T \leq T_2$ (Fig. 7.5b). The critical current in this range is very sensitive to the applied magnetic field, and shows a clear maximum at zero field along with structure

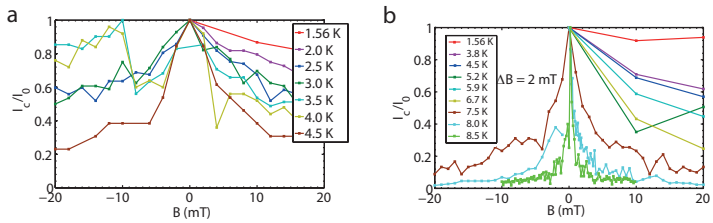

Figure 7.5: **(a)** Normalized I_c vs. magnetic field B for the 300 nm wide junction for different temperatures within the range $T \leq T_1$. The same is shown for the 50 nm for temperatures within the range $T \leq T_2$ in **(b)**.

suggesting side lobes with an oscillation period of ∼2 mT. Note that this period and the width of the central peak is comparable to the estimate given above, but smaller by about a factor of 4. For the effective area we need to include the London penetration depth of the $YBa_2Cu_3O_{7-\delta}$ superconductors on both sides, which is about 140 nm. Including the field penetration into the area we arrive at a new estimate of $\Delta B \simeq 1.2$ mT, which agrees quite well with the observed width of the peak. The fact that no more than 2 side lobes are visible per curve is an indication that the junction geometry is not sharply defined, which is also seen from the curved edges in the AFM images of Fig.7.3a. Given the limitations in the accuracy of the geometry, the agreement is quite good, and the experiment supports an interpretation of the junction as a Josephson coupling between the two $YBa_2Cu_3O_{7-\delta}$ superconductors, over a distance of 50 nm.

7.4 Conclusions

In summary, we report experiments on ion etched arrays of junction in bilayers of $La_{2-x}Sr_xCuO_4/YBa_2Cu_3O_{7-\delta}$ of widths varying from 50 to 300 nm. We show that it is possible to fabricate quasi *ab*-axis junctions by means Ar ion etching. A large T_c increase of the barrier material from 6.8 K to 9.0 K in the junction width of ∼ 50 nm is observed. The supercurrent in this junction geometry is preserved over a distance coinciding with ∼ 200 times the combined coherence lengths in the *c* and *ab* axes. The magnetic field measurements indicate clear difference in behavior of $I_c(B)$ between the 50 and 300

nm wide junctions, the former showing a clear main peak and several side lobes. These results support the Josephson junction-type behavior of the devices. The limitations in the accuracy by which the junction fabrication parameters, notably the etch depth profile, are known form the main obstacle for a more quantitative analysis.